

Physics and application of plasma diagnostics, electrostatic confinement and characterization by optical emission spectroscopy

Física e aplicação de diagnóstico de plasmas, confinamento eletrostático, e caracterização por espectroscopia de emissão óptica

Péricles Lopes Sant'Ana¹, Ana Catarina Freire², Michael Odstrcil², Roger Jaspers²

ABSTRACT

In this work, supplementary experiments were accomplished by using argon plasmas for studying in the field of nuclear fusion and plasma diagnostics. In this way, three attempts were accomplished to describe the physics of the probes, (plasma sheath), electrical breakdown and electro-static confinement assisted by Spectroscopy. (i) In the first attempt, Langmuir probes was aimed either to determine the electron density, temperature of the argon plasma, and the characteristic Current-Voltage curve (I-V). (ii) In the second attempt, the Paschen curve was acquired to demonstrate the effects that determine electrical breakdown in a gas, and then, it was possible determine the breakdown voltage. (iii) The last attempt, the electro-static confinement was analyzed using optical emission spectroscopy. The fusor has been suggested as a simple alternative to magnetic confinement. Although on fundamental grounds this claim cannot be supported, interesting physics aspects appeared, some of which have their counterpart in tokamak as well.

Keywords: Argon plasmas, Langmuir probes, Paschen curve, fusor, electro-static confinement, Optical Emission Spectroscopy.

RESUMO

Neste trabalho, experimentos complementares foram realizados usando plasmas de argônio para estudar no campo da energia nuclear, o diagnóstico de plasmas de fusão. Dessa forma, três experimentos foram realizados para descrever a física das sondas (na bainha do plasma), quebra dielétrica e confinamento eletrostático assistido por espectroscopia. (i) Na primeira tentativa, a sonda de Langmuir foi usada para se determinar a densidade de elétrons, a temperatura do plasma de argônio e a curva de corrente-tensão característica (I-V). (ii) Na segunda tentativa, a curva de Paschen foi adquirida para demonstrar os efeitos que determinam a quebra dielétrica em um gás e, em seguida, foi possível determinar a Voltagem em que ocorre a quebra dielétrica (iii) Na última tentativa, o confinamento eletrostático foi analisado usando espectroscopia de emissão óptica. A fusão foi sugerida como uma alternativa simples ao confinamento magnético. Embora, por razões fundamentais, esta afirmação pode não ser suportada, aspectos físicos interessantes apareceram, alguns dos quais têm contraparte em tokamaks.

Palavras-chave: Plasmas de argônio, sondas de Langmuir, curva de Paschen, fusão, confinamento eletrostático, espectroscopia de emissão óptica

1. Universidade Estadual de São Paulo – Sorocaba (SP) – Brazil

2. Technological University of Eindhoven – Eindhoven – Netherlands

Correspondence author: drsantanapl@gmail.com

Received: 05 Ago. 2019 **Approved:** 27 Ago. 2019

INTRODUCTION

Langmuir probe

An electrostatic probe was first used to measure the potential distribution in gas discharges on the ground by Joseph John Thomson. The theory was later developed by Irving Langmuir and his collaborators¹. The technique, with further developments, has been extensively applied to the study of gas discharges. A Langmuir probe refers to an electrode immersed in charged particle plasma, whose current–voltage (I – V) characteristics can be measured. From the I – V characteristics, one can estimate the temperature and number density of thermal electrons as bulk parameters which a DC bias is applied. The ideal I – V curve is demonstrated in Fig. 1.

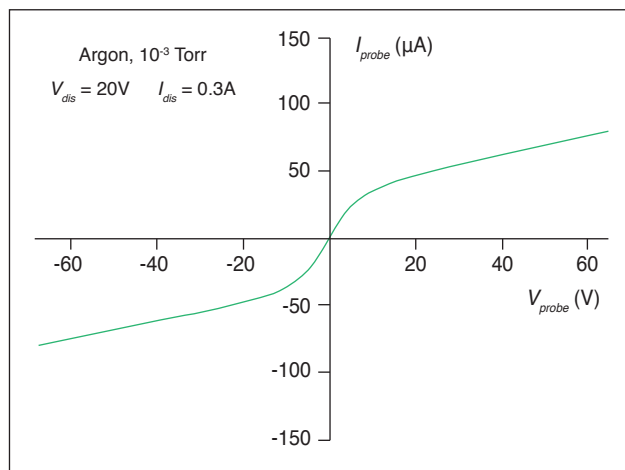


Figure 1: Typical double probe I – V characteristics in a nearly Maxwellian plasma (low discharge voltage, high argon pressure)².

In other studies, the effects of RF potential oscillation on the Langmuir probe characteristic I – V were described. This method is based on using a time-averaged Langmuir probe I – V characteristics³. The I – V characteristics has three different regions: 1) ion saturation region where the electrons are repelled but ions are collected; 2) electron retarding potential region where most of the current is due to electrons, but the actual current is determined by the number of electrons which can overcome a retarding potential; and 3) electron saturation region where ions are repelled but electrons are attracted to the probe. The probe leads were shielded by bare metal tubes to eliminate RF interferences in the probe circuits as has been done in previous research⁴.

When a probe is immersed in plasmas, its current generally depends on the collections of positive ions, negative ions, and electrons. We consider the electron current on a spherical probe under the condition that the electrons have a Maxwellian velocity distribution in a coordinate system fixed with respect to the probe. Recent studies report the use of tungsten filament (probe) for plasma diagnostics⁵. Other work⁶, also was dedicated to probe measurements in RF plasmas using bare metal protective shields underneath the floating potential.

For understanding, developing and maintaining plasma processes, it is desirable to determine the basic plasma parameters⁷, like electron temperature, plasma density and their dependence on the discharge voltage and operating gas pressure. Nowadays, it was reported in literature the use of Langmuir probe to measure these parameters⁸.

Electron plasma parameters such as density, temperature and the energy distribution depend on the plasma operating conditions such as gas composition, pressure, applied power, reactor geometry and reactor material⁹.

In recent studies, standard probe measurements were determined to registering the following parameters of plasma: electron temperature (T_e), electron concentration (n_e), floating potential of probe (V_f), potential of space (V_s), and its corresponding density of electron saturation current (j_{es}). These parameters quite sufficiently characterize the physical state of plasma¹⁰. In addition, other studies considered the particle mass (m_p)¹¹ as an important parameter.

There are several factors which may prevent accurate measurement of electron temperature and density in plasmas by Langmuir probes. Among them, a contamination of the probe surface is one of the most potential sources of error. In particular, the electron temperature tends to be estimated to be higher than the true value when the probe has a contaminated surface. Hysteresis in the measurement of I – V characteristics may also be seen in such a situation¹².

In general, the electron current is calculated by subtracting the ion current from the probe current, where the ion current is estimated by extrapolation from the ion saturation current. Electron current is completely controlled by the ion saturation current so that probe draws very little amount of current without disturbing the plasma conditions^{13,14}.

The electron temperature is estimated from the gradient, which is proportional to $1/T_e$, in a plot of $\log(I_e)$. The random electron current is a function of the electron temperature and density. Therefore, once the random electron current and the electron temperature are known, the number density of electrons can be calculated. In other recent studies, it was noted that parameters such as the electron density and the electron temperature can also be obtained from the electron energy probability function (EPPF)¹⁵. More recent studies can be found in literature^{16–19}.

An investigation into the referencing limitations of probe was presented by Babu²⁰, however, it is rarely observed in argon plasmas. For another gas, recent studies reported its dielectric properties using Langmuir Probe^{21–24}.

Paschen curve

The electric breakdown of gases is one of the fundamental phenomena of gas discharge physics. It has been studied for a long time but still attracts incessant interest of researchers²⁵. Besides the interesting physics, breakdown is important for many applications including development of reliable electric insulation

in electric grids and the study of different aspects of gas discharge physics^{26,27}. Normally, a breakdown is represented by the so-called Paschen curve or the Paschen law²⁸.

The electrical breakdown occurs in Townsend regime when the ions reaching the cathode have sufficient energy to generate secondary electrons²⁹. The reflection of electrons from the plasma volume walls is important in gas discharge physics. For example, this effect may have profound influence on probe measurements³⁰. The ion-assisted field emission takes over in this regime and lowers the breakdown voltage considerably³¹.

The breakdown voltage (V_b) for a particular gas and electrode material depends on the product of the pressure and the distance between the electrodes, as expressed in Paschen law. This breakdown voltage curve represents a balance between the number of electrons lost by diffusion and drift in the interelectrode gap and the number of secondary electrons generated at the cathode³².

V_b increases as pd increases on the right side of the Paschen curve and increases with respect to the lowest breakdown value on the left side of the Paschen curve. For most gases, V_b is a single-valued function of pd . At high pressures, breakdown voltage follows Paschen law until the electric field reaches the critical value and, after that, breakdown curve falls below the pure Paschen curve³³.

For the breakdown, failures from the Paschen law are observed in different regions³⁴. First, departure appears at the right-hand branch of the curve corresponding to high pressures. The deviation is also noticed at the left-hand branch related to the low pressures and finally near the minimum of the breakdown curve. For each region, the required value for the electric field has to be of the order of 10^6 V.cm⁻¹ or more to induce a field emission effect from the cathode.

The critical issue in extending the standard (gaps of distance $d = 1$ cm, and pressures $p = 1$ Torr) low pressure discharges to dimensions of the order of millimeters is how to predict the conditions that could lead to a breakdown³⁵. In this way, we prefer to regard the Paschen curve (law) as the dependence of the breakdown voltage on pd (the pressure-gap product) without implying any analytic dependences³⁶. It was found that when the additional electron emission due to the high electric field is included, the breakdown voltage decreases very rapidly with decreasing pd (for smaller pd) of the Paschen minimum. However, in a number of papers, experimental Paschen curves obtained for both DC and rf discharges displayed a plateau to the minimum and these curves disagreed with those obtained at standard dimensions^{37,38}.

In other study, the higher pd values the scaling of electrical characteristics and light emission intensity with electrode separation was verified³⁹. Figure 2 shows a typical Paschen curve for a given gas, where the breakdown voltage (V_b) was fitted as function of pressure \times distance (pd).

Other authors also reported that Paschen law predicts the value of the breakdown voltage as a function of the product of

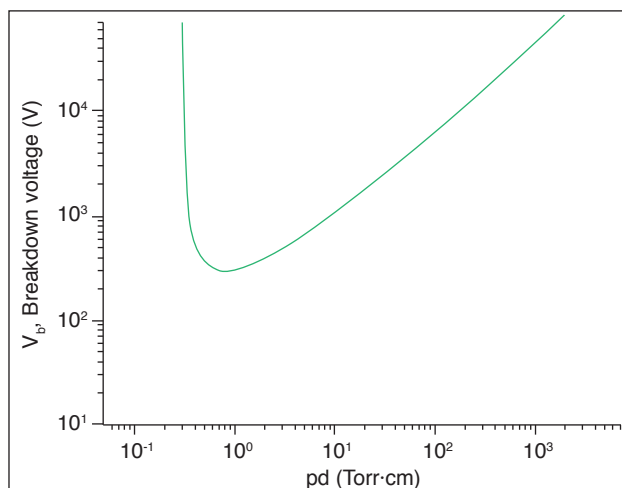


Figure 2: Typical Paschen curve. Breakdown voltage V_b (the voltage at which the plasma begins to arc) as function of pressure \times gap distance (pd)⁴⁰.

the pressure and the interelectrode distance, $V_b = f(pd)$ in a given gas for a given reactor configuration⁴¹.

An additional and independent influence of the interelectrode distance on the breakdown voltage has been observed by Penning and Addink⁴², Miler⁴³, Auday et al.⁴⁴, Lisovskiy et al.⁴⁵, and Mariotti et al.⁴⁶.

Moreover, breakdown voltage curves corresponding to the measured breakdown voltages for RF discharges in argon and DC discharges with various electrode materials can be found in another study⁴⁷. Under the same discharge conditions (including capacitor voltage, cathode material, shape and electrode spacing), the electrode configuration with higher breakdown voltage is able to generate higher-density plasma since the cathode runaway electrons can gain relatively larger energy from the electric field⁴⁸. In addition, the DC breakdown voltage curves in argon discharges for different gap spacing is described in literature⁴⁹. Recent studies also revealed the voltage breakdown as function of product (pd) and Paschen curve using argon plasma for a distance $d = 2$ cm, while the pressure was changed from 0.4 to 2.6 mbar⁵⁰.

Fusor (electrostatic confinement)

Atomic spectra are known to be a rich source of information about the structure of atomic nuclei without involving any model concepts. It was shown that spectroscopic methods may appear very promising for this kind of investigation⁵¹. Later, natural spectral-line broadening in atoms with unstable nuclei was explored by Gainutdinov⁵².

Spherical electrodes immersed into background plasma were first studied by Stenzel et al.^{53,54}. In these two companion papers, the bias on the relevant electrode was positive with respect to ground. In this way, electrons can oscillate between the boundaries of the gridded anode. The main difference between the aforementioned works and this third experiment is that the sign for the electrode bias in this work is highly negative. Its amplitude is in fact so high

that the ions can gain enough kinetic energy to undergo fusion reactions. Fig. 3 shows schematic of a possible experimental setup.

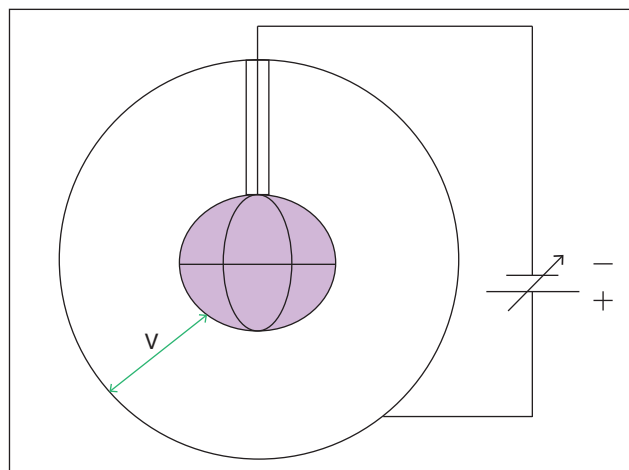


Figure 3: Schematic of a possible experimental setup. Ions are accelerated by the applied voltage into the grid in the center of the machine where they are able to fuse⁵⁵.

Generally, spectral diagnostic methods attempt to establish relationships between the plasma parameters and the radiation features, such as the emission or absorption intensity and the broadening or shifting of the spectral lines⁵⁶. An emission line is defined as the energy emitted per second and it depends on the probability of transitioning between the two involved energy levels and their electron population.

Several factors result in the broadening of the spectral lines. In the following, the most important factors for broadening are explained⁵⁷.

The spectral lines are not infinitely sharp in wavelength or frequency, but has a spread in wavelength/frequency described by a Lorentzian profile. Hutchinson⁵⁸ noted that spectral lines emitted by bound-bound transitions do not have an infinitesimal spectra width, but undergo several possible lines broadening mechanism useful for diagnostics.

Many studies in the literature on plasma parameters use the optical emission spectroscopy (OES) technique, which can be applied in many fields, from spatial plasmas⁵⁹ to laboratory experiments, such as in nuclear fusion⁶⁰.

OES is the most popular technique to investigate glow discharges since it is simple and produces no perturbation in the plasma⁶¹. Some authors⁶² also have used OES for probing the cold plasma (few eV electrons), whose role is relevant in plasma stability. Nevertheless, OES is used to measure vibrational, rotational and gas temperatures⁶³ and electron energy distribution functions (EEDFs)⁶⁴ in argon plasmas. Moreover, the optical emission spectrum of capacitive and inductive discharge has been compared in detail⁶⁵. Fig. 4 shows the background line broadening for our experiments.

Recently, it was developed a nonequilibrium collisional-radiative model (CRM) for pure argon to calculate the populations

of argon excited states and line intensities⁶⁶. In particular, they focused on the light emission of the three most intense argon atomic lines at 811.5 nm, 763.5 nm, and 750.4 nm.

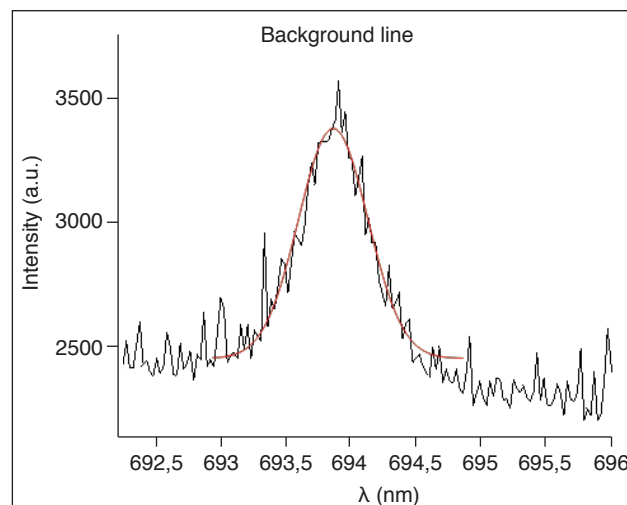


Figure 4: Background broadening acquired by optical emission spectroscopy (OES) for argon under -10 kV and 3.2×10^{-3} mbar.

From OES measurements reported in the literature, it is known that the relative intensity of these dominant argon lines depends on the type of plasma. In capacitively coupled plasmas (CCP)⁶⁷, inductively coupled plasmas (ICP)⁶⁸, and glow discharges⁶⁹, the 811.5 nm line is the dominant line in pure argon. For glow discharges⁷⁰, and CCP plasmas^{71,72}, the relative increase in emission intensity is $811.5 \text{ nm} > 763.5 \text{ nm} > 750.4 \text{ nm}$. In ICP plasmas^{73,74}, the intensity of 750.4 nm line is reported to be higher than the 763.5 nm line.

In pure argon, the 811.5 nm line presented the highest intensity because it originates from the 2p9 state, which is the most populated level. It is followed by the 763.5 nm line, which originates from the 2p6 level with the second highest population, and finally, by the 750.4 nm line, which originates from the least populated 2p1 state⁷⁵.

The electron impact excitation cross sections out of the argon ground state are taken from literature⁷⁶. The electron impact excitation rates out of the argon ground state account for direct excitation only. The total rates, however, include cascades from higher lying levels.

Emitting atoms suffer frequent collisions with other atoms and ions in the plasma, which produces distortion of their energy levels. This is a mechanism leading to the so-called collisional broadening of the emission lines. Depending on the nature of disturbing particles, there are different types of collisional broadenings: Van der Waals, resonance and Stark broadenings.

The Van der Waals broadening is due to dipole moment induced by neutral atom perturbers in the instantaneous oscillating electric field of the excited emitter atom⁷⁷. The resonance broadening of spectral lines is due to dipole-dipole interactions of the emitter with ground-state atoms of the same element^{78,79}.

The Stark broadening results from Coulomb interactions between the emitter atom and surrounding charged particles, perturbing the electric field it experiences. Both ions and electrons induce Stark broadening, but, in nonthermal plasmas, electrons are responsible for the major part of it because of their higher relative velocities⁸⁰.

These three collisional broadenings mechanism generates a Lorentzian shape profile with a FWHM for argon.

EXPERIMENTAL

In the first attempt (i), an insulating probe with tungsten electrode tip was positioned in argon plasma. A voltage stepping between a lower and upper limit was applied between the probe tip and the plasma. The tips measured 19×10^{-3} and 3×10^{-3} m. The area was 1.3273×10^{-4} m. The current running from the electrode to the plasma was recorded and the I-V was fitted to determine plasma temperature and density. The source 300 VDC was applied to an alternative electrical configuration, the pressure in the chamber was 8.0×10^{-5} bar. The series resistors reached $1.2 \times 10^3 \Omega$ and the maximum current (i_{max}) reached 100×10^{-3} A. The computer-controlled probe was calculated using a "Keithley 2400" source meter from Tektronix Company.

In this second attempt (ii), an argon plasma was used to record the breakdown voltage as a function of pressure and distance between the electrodes until the saturation of electrical current using a DC power supply. In the first step, the argon pressure was changed from 0.08×10^{-3} to 47.4×10^{-3} bar, while the distance between the electrodes was fixed to 3.6×10^{-3} m. The voltage applied was changed from 3.2×10^3 to 2.6×10^6 V, while the output current was 4×10^{-3} A. The objective was to fit the curve voltage \times pressure. In the second step, the pressure was fixed at 1×10^{-3} bar and current 4×10^{-3} A, while voltage was changed from 260 to 500 V, in order to collect the voltage \times distance curve. Figure 5 shows the scheme of experimental plasma system for i and ii.

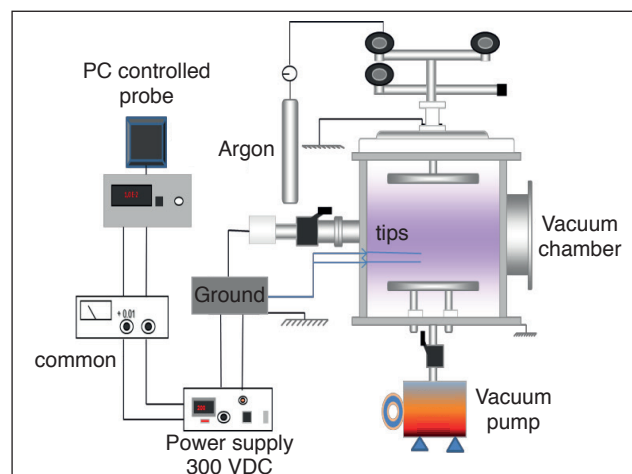


Figure 5: Scheme of experimental plasma system for i and ii. The diameters of the tips are: $\varnothing = 3$ mm and $\varnothing = 19$ mm. The PC-controlled probe was a "Keithley 2400".

In the third attempt (iii), another plasma system was used for the electrostatic confinement, which was accomplished in a self-build fusor experiment consisted in a spherical vacuum chamber with diameter of 50×10^{-2} m, containing an internal grid at -100×10^3 V potential in a low electrical current of $\sim 15 \times 10^{-3}$ A, using argon plasmas in a pressure work of 3.2×10^{-6} bar. The measurements of plasma parameters were acquired using OES and density profile was determined. It was possible to fit the four spectral lines of optical emission from temperatures between 7 to 10 eV.

The underlying concept is rather simple: a high voltage of several kV (up to several hundred kV) accelerates ions from background plasma radially into the inner grid electrode where they collide and fuse. The frequently used working gases are a mixture of deuterium and tritium or pure deuterium gas, which is not, was available.

The scheme of experimental plasma fusor system for iii can be observed in Fig. 6.

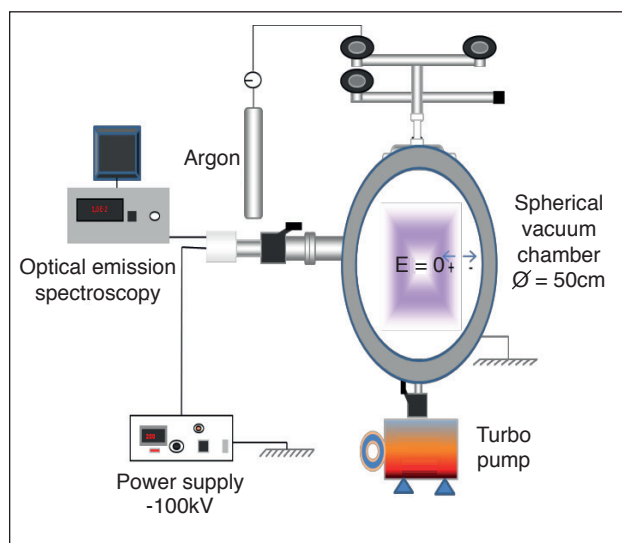


Figure 6: scheme of experimental plasma fusor system for iii. Argon ions are accelerated by the applied negative voltage of -100 kV into the grid in the center of the reactor.

The argon gas was used as an alternative for the iii experiment. For this experiment, it is assumed that the system does not present a perfect spherical symmetry; it is possible to obtain grid loss energy collision losses, and finally, at center, the electric field ($E \neq 0$).

RESULTS AND DISCUSSIONS

Langmuir probe and optical spectroscopy were recently studied⁸¹ using argon plasma⁸². Argon gas is considered as one of the most often used gases in plasma technologies. The relative cheapness of argon also enables it to be used as the carrier gas in industry⁸³. The results and discussions are presented for the three experiments (i, ii and iii):

Experiment i

The electron density and temperature are the basic parameters that characterize space plasmas; they were obtained through *in situ* measurements by using Langmuir probes, which is in agreement with recent studies⁸⁴. The I–V characteristic can describe the operating regime of the electric discharge. Using this I–V curve, the plasma parameters of interest can be calculated⁸⁵. To obtain the I–V characteristic, the power supply voltage was varied for a top current of 2.8×10^{-6} A, in an area of 1.3273×10^{-4} m, while the argon pressure was 1.338×10^{-3} bar.

The real current saturation cannot be estimated for this range. Thus, the curve represents the transition region between electronic and ionic current saturation. In this region, while the electric field is very small, the value of the current (some tens of μ A) will be proportional to the rate at which the ions and electrons move toward the electrodes. Under these conditions, the density of current is proportional to the electric field and the voltage range, reaches some tens of volts, and independently of how potent is the power source. Fig. 7 shows the results obtained in this study.

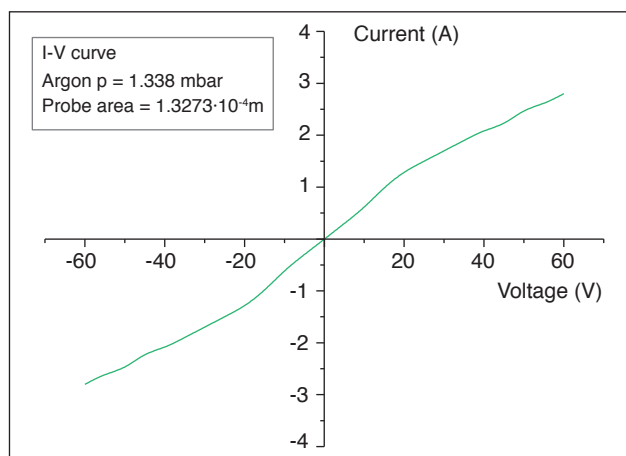


Figure 7: I–V curve resulted from i experiment.

At 1.338×10^{-3} bar (~ 130 Pa), the random flux (Γ) of argon atoms (a.m.u 40) at room temperature is 2×10^{25} atoms $\text{m}^{-2}\cdot\text{s}^{-1}$. The distance travelled by an argon atom between collisions will be on average about 0.11×10^{-3} m, and the frequency of collisions between gas atoms at room temperature is 3.5×10^6 s^{-1} ⁸⁶. The linearity observed on the graph is interpreted as follows: as long as the electric field is very small, the equilibrium between the production and the loss of charge in the medium will be maintained and the current value will be proportional to the speed with which the ions and electrons move towards the electrodes. Under these conditions the current density is proportional to the electric field and, consequently, the phase is an ohmic conductor.

On the other hand, the ranges of data collection from current and voltage were not sufficient to fit the curve as the I–V curve described in Figure 1, thus the fitted curve is quite linear in this range for those plasma conditions. It is suggested that the probe currents in this experiment were saturated at the maximum

voltages of 60 and -60 V. Thus, the plasma potential should be smaller than 60 V because the electrons moved from the plasma to the probes by the electric force of the applied saturation voltage.

Extrapolating this region, the plasma discharge will be in progress, thus, when the bias voltage on the probe reaches a sufficiently negative value with respect to the plasma potential, the probe collects the ion saturation current. Positive ions continue to be collected by the probe until the bias voltage reaches the plasma potential; at this point, ions begin to be repelled by the probe. If the bias voltage is higher than the plasma potential, all positive ions are repelled, and the ion current to the probe vanishes⁸⁷. Similarly, when the probe is positively biased, then most of the current to the probe is due to electrons, but the actual current is determined by the number of electrons overcoming a retarding potential⁸⁸.

Other works review probes in flowing plasma conditions at moderate to high pressures^{89,90}. At higher pressures ($p > 50$ Pa), the frequency of electron collisions with the plasma species also increases and the mean free path between successive collisions decreases. It shows that the electrons lose their energy in the discharge. Thus, as the chamber pressure increases, more and more energy is transferred from the electrons to the plasma species.

In addition, the elastic collisions of electrons with the plasma species can also play a significant role in reduction of ionization events. Similarly, at higher pressures, the high-energy tail depletes to low energies; as a result, the availability of highly energetic electrons for electron impact ionization processes and, consequently, the electron number density (n_e) decreases. This depletion in the tail of the electron energy distribution function might be due to rapid diffusion and recombination of highly energetic electrons at the chamber walls^{91,92}.

At low pressure, when mean free paths are relatively long, the electrons remain much hotter than the gas; conversely, at high pressures, thermal equilibrium can be approached. A crude estimate of the electric field in a self-sustaining plasma can be obtained by supposing that electrons travel their entire free path in the direction of the field and lose all the energy gained in an optimum collision with the (cold) gas, (which suggests a scaling of temperature with E/p). This gives several volts/cm at next to 1 Torr in argon (133.32 Pa).

Experiment ii

If an electric field is applied to a plain parallel gap of width (d), containing a gas, at sufficiently high fields, the gas suddenly switches from being insulating dielectric to conducting gas. It is supposed that a few electrons are always around in the gap, either by the action of cosmic rays or else as a consequence of field emission from asperities on the surface, close to which electric fields are strongly enhanced. Our results are consistent with the theory^{93,94} that predicts the violation of scaling when field emission becomes significant only at gaps smaller than 10 μm .

Our plasma reactor is designed in a DC configuration, and has two electrodes “cathode and anode”, with an adjustable interelectrodes distance; the maximal interelectrodes spacing is approximately calculated. Fig. 8 shows the results of voltages as function of pressure, and voltage as function of electrode distance.

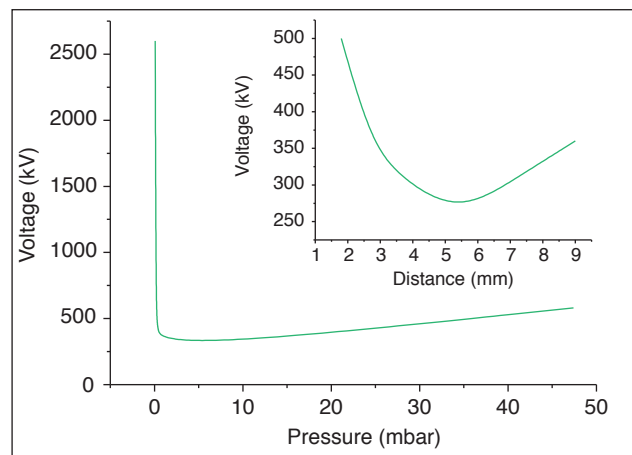


Figure 8: Graph of voltage applied (kV) as function of argon pressure (mbar) spectral emission lines resulted from experiment ii, enclosed to the graph of voltage (kV) as function of electrode distance (mm).

]The gap between the electrodes, so the electrons cannot gain enough energy to perform ionizations. Consequently, a higher voltage is required to assure ionization of enough argon gas atoms to start an avalanche. Argon is monoatomic and tends to have smaller diameters and, therefore, a greater mean free path length. Figure 9 shows the Paschen curve as result of the experiment ii⁹⁵.

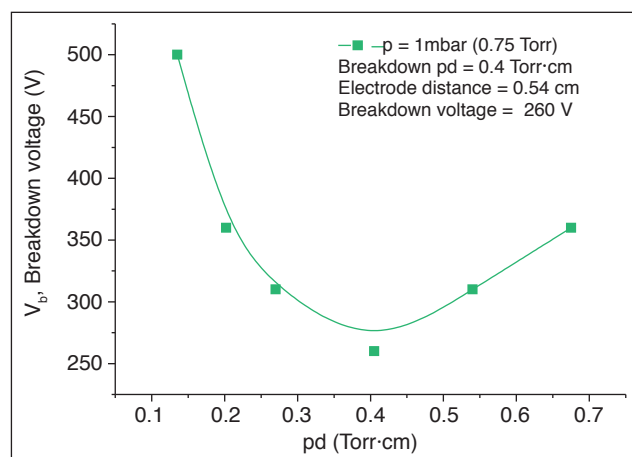


Figure 9: Graph of V_b , breakdown voltage (V) as function of argon pressure (Torr) \times electrode distance (cm), which represents the Paschen curve for experiment ii.

The shape of the curve can be attributed to the increase of collision on the left side and decrease of ionization cross section on the right side⁹⁶.

To determine the breakdown threshold, the electric field distortion can be neglected, and the field can be assumed uniform and equal to the applied field⁹⁷. As with DC (and low-frequency)

breakdown, higher values of pd require larger voltages to achieve breakdown, and at low pd there is again a sharp rise in breakdown voltage. For a pressure of 1 mbar (0.75 Torr), the minimum breakdown voltage (V_b) is 260 V.

If the long path explanation is considered then, the penetration of the discharge into the gap between the electrode and the insulator allows the discharge length to vary as required and the breakdown voltage stays close to the minimum value⁹⁸.

Experiment iii

The total collisional broadening result from the convolution of sum of the three mechanisms (Van der Waals, Resonance and Spark broadening).

The Lorentzian line shape typical of natural broadening: $I(v) = (1 + \Delta v^2)^{-1}$, with Δv in units of $1/2\Gamma t$, where t is the lifetime of argon atom in an upper state. This arises straightforwardly from the Doppler shift caused by thermal argon particle motion. The thermal Doppler broadening is one of the explanations for the broadening of spectral lines. Figure 8 shows the spectral emission lines from 4×10^{-3} mbar of argon plasma under -10.0 kV and 15 mA. In addition, the energies for fusor are 17.6 and 91.1 MeV. Fig.10 shows the image of the spectral emission lines from argon plasma.



Figure 10: Photography of argon spectral emission lines resulted from experiment iii by applying of -10 kV, $I = 20.2$ mA and 4×10^{-3} mbar.

Different velocities of the argon particles emission result in different Doppler shifts, the cumulative effect of which is the line broadening⁹⁹.

Table 1 shows the values of retrieved parameters acquired by OES.

In general, the production processes of excited species include the electron-impact excitations from the ground and from the metastable states, the radiation decay from the higher excited states, etc. The following calculations are based on the assumption that the plasma between the two spherical electrodes is collisionless (this is reasonable because most of such electrostatic confinement fusion experiments are carried out at a pressure

around 10^{-6} bar, where the mean free paths are in the order of the size of the machine).

The spectral lines emitted by bound-bound transitions do not have infinitesimal spectral width, but undergo several possible line broadening mechanisms that are extremely useful for diagnostics. The energy spread arises because perturbations of the atomic system due to interaction with the electromagnetic fields of virtual (or real) photons cause the quantum states to be only approximate eigenmodes of the system. The temperature was measured for different potentials. For each applied potential, the wavelength resulted to the same peaks formation, around 420 ± 0.5 and 528 ± 0.5 nm.

Figure 11 shows the broadening lines for argon temperatures from 7 to 10 keV. The spectrum of intensity lines is showed as function of wavelength (nm).

The moderated fields act not to split the upper emitting state, but it rather acts to broaden the emitted line. It was shown earlier that this effect leads to inhomogeneous broadening of spectral line, i.e., the emitted line becomes of Lorentzian shape on contrast to other broadening mechanisms, e.g. Doppler effect, which leads to a homogeneous broadening¹⁰⁰.

In recent literature, a method to circumvent this dependence on electron density by considering pairs of emitted lines was proposed. This method allows the determination of the gas

Table 1: Values of data acquired by optical emission spectroscopy from argon plasma with $E = -10$ keV, $I = 20.2$ mA and $p = 4 \times 10^{-3}$ mbar.

Lines/energies	Area	Center	Width	Offset
Cosmic line	-84958	648.34	323.06	856.11
Line 696 (Background)	-32750	691.72	19.72	3772.9
T = 7 keV	-1.737 E-6	528.5	325.61	5905.2
T = 8 keV	-1.7375 E-6	528.5	325.6	5805.2
T = 9 keV	-1.704 E-6	527.85	319.7	5895.7
T = 10 keV	-1.06 E-6	528.97	313.107	4356.0

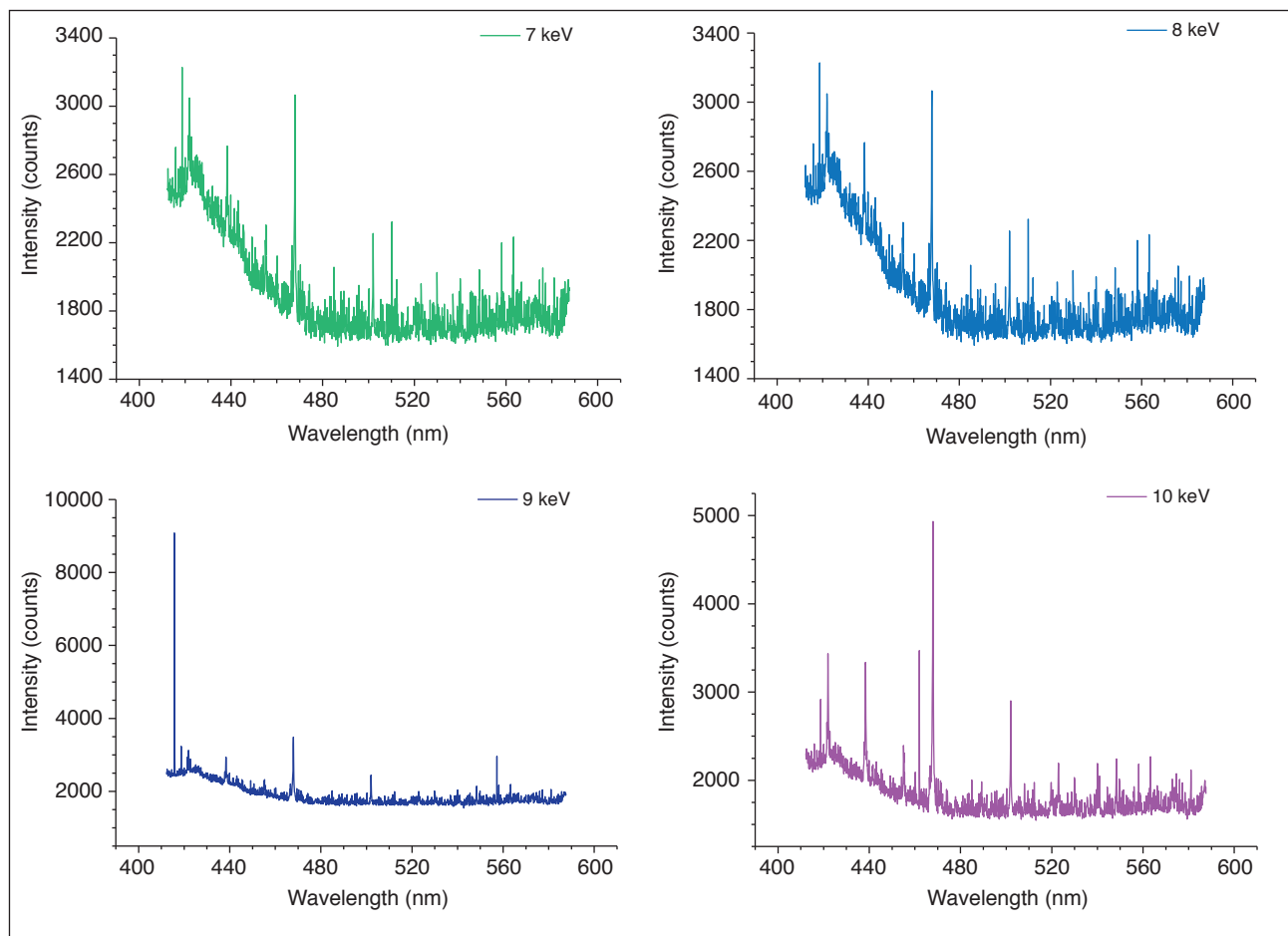


Figure 11: Spectrum of lines broadening from argon plasma resulted from experiment iii by applying -100 kV and 3.2×10^{-3} mbar, in different temperatures.

temperature from the measurements of Lorentzian profiles of some pairs of argon atomic lines, and when applying it, no assumptions on the degree of thermodynamic equilibrium among excited states are needed¹⁰¹.

For thermal plasmas with a gas temperature similar to the electron one, the mobility of ions is high and the impact approximation is also valid for ions, being their contribution to the broadening also being Lorentzian. In the ion impact limit, line profiles are symmetric Lorentzian. On the contrary, for plasmas where the ion mobility is small (e.g., plasmas with gas temperature relatively low), a quasistatic approximation is often needed to model the ion broadening in order to explain the slightly asymmetric shape of the profiles. The less dynamical the ions are, the more asymmetric the lines are.

Finally, Fig. 12 shows the spectrum of lines emission from argon plasmas resulted from experiment iii by applying of -10 kV and 3.2×10^{-3} mbar for different temperatures.

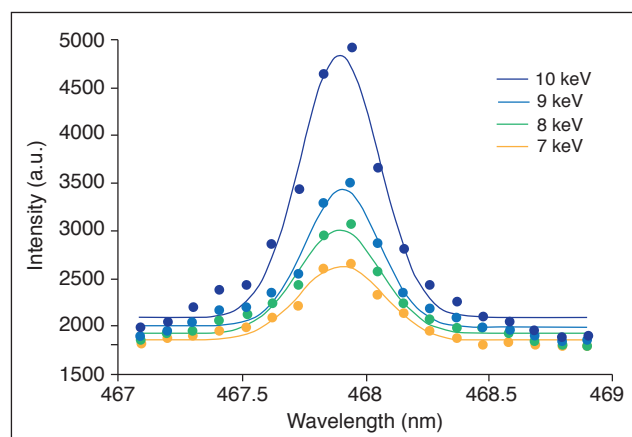


Figure 12: Lorentzian Spectrum of argon plasma resulted from iii experiment by applying of -10 kV and 3.2×10^{-3} mbar.

The 4 peaks ranged between 467 and 469 nm. The peaks of line broadening to argon comprise ions excitation (electronic transitions). While the fusor is in progress, the spectra intensity (counts) will change, and then it is possible to determine the temperature (ΔT) in the plasma. The data were collected applying high voltage of -10 keV while top current was 20.2 mA.

The intensity of these lines is obtained from the spectrum by taking integration over the respective profiles and normalizing the same with the spectral response of the instrumental sensitivity.

The spectra emitted from plasma contain a wealth of information that are stored in the emitted line shape as well as the continuum radiation often appeared under the emitted lines. The relative spectral radiance (in the units of counts per second) of some emitted lines can be related to the plasma temperature, while the Lorentzian full width of the line at half of the maximum spectral radiance (FWHM) usually contains information about electron and/or ion density¹⁰²⁻¹⁰⁴.

The described discharge operation of argon is found in literature¹⁰⁵. They developed the volume averaged global model for

low-pressure high-density discharges for noble gases, including argon. While argon ions are moving a Maxwell-Boltzmann distance ($\Delta d = d - d_0$), there are photon emission with initial velocity (v_0) to final velocity (v_f) due to energy loss.

Analyzing the FWHM, it can be estimated for each temperature with the equation $\Delta d = \lambda_2 - \lambda_1 \approx 0.20 \pm 0.1$ nm. Using the equations $d/d_0 = (1 - v/c)$, and $\Delta f = v/d_0$, then, the estimated electrons frequency is 2.1363 MHz. The distance Δd does not change significantly for each condition, which means that the temperature does not change significantly as function of the applied ΔV .

Measuring the temperature (T_e) of thermal electrons and number density (n_e) of thermal electrons in the argon plasma

Input:

$$m_{\text{argon}} = 40 \times 1.27 \cdot 10^{-27} = 6.4 \times 10^{-26} \text{ kg.}$$

$$c = 3 \times 10^8 \text{ m/s}^{-1} \text{ (light velocity in vacuum)}$$

$$\lambda_{\text{argon}} = 467.9 \times 10^{-9} \text{ m (spectral line position peak)}$$

For $E_1 = 17.6$ MeV (typical fusor energy):

$$1 \text{ eV} = 1.6 \times 10^{-19} \text{ J}$$

$$17.6 \times 10^6 \text{ eV} = x \text{ J}; \text{ then } x = 2.816 \times 10^{-12} \text{ J}$$

Velocity:

$$V_{01} = [(2.816 \times 10^{-12} \text{ J} \times 467.9 \times 10^{-9} \text{ m}) / 6.64 \times 10^{-34} \text{ J s}]^{1/2}$$

$$V_{01} = 3.92 \times 10^7 \text{ m.s}^{-1}.$$

For $E_2 = 911$ MeV (fusor energy):

$$\text{neutronicity} = 0.8$$

$$\text{and power density} = 34 \text{ W/m}^3/\text{kPa}^2$$

$$1 \text{ eV} = 1.6 \times 10^{-19} \text{ J}$$

$$911 \times 10^6 \text{ eV} = x \text{ J}; \text{ then } x = 1.457 \times 10^{-10} \text{ J}$$

Velocity:

$$V_{02} = [(1.457 \times 10^{-10} \text{ J} \times 467.9 \times 10^{-9} \text{ m}) / 6.64 \times 10^{-34} \text{ J s}]^{1/2}$$

$$V_{02} = 1.01 \times 10^8 \text{ m.s}^{-1}.$$

Using the equation 6.4.8 p. 265,¹⁰⁶. The results showed that:

$$E/h = \Delta v_{1/2} = 2v_0 (v_{ta}/c) (2 \ln 2)^{1/2}; v_{ta}^2 = T_{\text{argon}}/m_{\text{argon}}$$

Where: $\Delta v_{1/2}$ is the full-width at half-maximum of the Lorentzian:

For $E_1 = 17.6$ MeV:

$$17.6 \times 10^6 \text{ eV}/6.64 \times 10^{-34} \text{ J s} = 2 v_{01}^2 [(T_1/m)^{1/2} \times 1/c] (2 \ln 2)^{1/2}$$

$$2.65 \times 10^{40} \text{ eV/J s kg s}^{-1} = 4.63 \times 10^{15} \text{ m.s}^{-1} [(T_1/m)^{1/2} \times 1/3 \times 10^8 \text{ m.s}^{-1}]$$

$$1.71 \times 10^{33} = (T_1/m)^{1/2}$$

$$4.14 \times 10^{16} = T_1/m$$

$$T_1 = 4.14 \times 10^{16} \text{ eV/kg} \times 6.4 \times 10^{-26} \text{ kg} = 2.65 \times 10^9 \text{ eV}$$

$$T_1 = 2.65 \times 10^{-9} \text{ eV} \times 17.6 \times 10^6 \text{ eV} = 0.046675 \text{ eV}^2$$

$$T_1 e = 0.21 \text{ eV} = 2507.41 \text{ kelvin} = \Delta\lambda \text{ Gaussian} = d - d_0$$

$$\text{Where: } E(v) = A \exp [-0.5mv^2/T]$$

$$\text{For } E_2 = 911 \text{ MeV:}$$

$$911 \times 10^6 \text{ eV} / 6.64 \times 10^{-34} \text{ J s} = 2 v_{02}^2 [(T_2/m)^{1/2} \times 1/c] (2 \ln 2)^{1/2}$$

$$1.37 \times 10^{42} \text{ eV/J s kg s}^{-1} = 2.38 \times 10^{17} \text{ m/s} [(T_2/m)^{1/2} \times 1/3 \times 10^8 \text{ m.s}^{-1}]$$

$$1.73 \times 10^{33} = (T_2/m)^{1/2}$$

$$4.15 \times 10^{16} = T_2/m$$

$$T_2 = 4.15 \times 10^{16} \text{ eV/kg} \times 6.4 \times 10^{-26} \text{ kg} = 2.66 \times 10^{-9} \text{ eV}$$

$$T_2 = 2.66 \times 10^{-9} \times 911 \times 10^6 \text{ eV} = 2.4228 \text{ eV}^2$$

$$T_2 e = 1.55 \text{ eV} = 18065.41 \text{ kelvin} = \Delta\lambda \text{ Gaussian} = d - d_0$$

$$\text{Where: } E(v) = A \exp [-0.5mv^2/T]$$

$$\text{Analogously, for } E_3 = 931 \text{ MeV:}$$

$$T_3 = 1.58 \text{ eV} = 18368.72 \text{ kelvin} = \Delta\lambda \text{ Gaussian} = d - d_0$$

$$\text{Where: } E(v) = A \exp [-0.5mv^2/T]$$

For this Te ranges (1.55 eV to 1.58 eV), the number density (ne) of thermal electrons can be calculated using the equation:

$$ne = \Gamma / [kT/2\Pi m]^{1/2}$$

Where:

Γ = random flux of argon atoms at room temperature [2×10^{25} atoms \times m⁻² \times s⁻¹]

$$K = \text{Boltzmann} [8.617 \times 10^{-5} \text{ eV m}^2 \text{ kg/s}^2 \text{ k}]$$

$$\Pi = 3.14$$

$$m = \text{argon mass [kg]}$$

$$ne = 2 \times 10^{25} / [8.617 \times 10^{-5} \times 18150 / 2 \times 3.14 \times 6.4 \times 10^{-26}]$$

$$ne = 2 \times 10^{25} / 1.97 \times 10^{12}$$

$$ne = 1.012 \times 10^{13} \text{ m}^{-3} \sim 10^{13} \text{ m}^{-3}$$

Using the breakdown voltage (Vb) for calculate Townsend coefficient of argon ionization

Moreover, the Paschen law was used to calculate the breakdown voltage (Vb). In this case, the equation can be found in¹⁰⁷.

$$Vb = B p d / \ln(Apd) - \ln[\ln(1 + 1/\gamma)]$$

Where:

$$P = \text{argon pressure} = 100 \text{ Pa}$$

$$d = \text{electrode distance (m)} = 5.4 \times 10^{-3} \text{ m}$$

$$Vb = 260 \text{ V.}$$

γ = Townsend coefficient of argon ionization, which represents the number of electrons produced by secondary processes, that explain the increase of ion current during the increase of the

voltage, followed by relaxed electric field. (The higher efficiency of secondary ionization processes in argon discharge occurs in the region of the Paschen's minimum; in this case, next to 260 Vb).

A [Pa⁻¹ cm⁻¹]; B [V Pa⁻¹ cm⁻¹] are constants, supposed to be:

$$1^\circ \text{ attempt: } A = 1.5 \text{ for } B = 0.0984$$

$$\text{then, } \gamma = 0.172$$

$$2^\circ \text{ attempt: } A = 4.14 \times 10^{-3} \text{ for } B = 1.57 \times 10^{-4}$$

$$\text{then, } \gamma = 0.60$$

$$3^\circ \text{ attempt: } A = 0.09 \text{ for } B = 1.35$$

$$\text{then, } \gamma = 0.00386$$

CONCLUSIONS

For experiment i, with the data collected from I-V curves, provided to the region of the linear fit, was not possible to estimate the real current saturation. A crude estimate of the electric field in a self-sustaining plasma can be obtained by supposing that electrons travel their entire free path in the direction of the field and lose all the gained energy in an optimum collision with the (cold) gas, (which suggests a scaling of temperature with E/p). This gives several volts/cm at 1 Torr in argon (133.32 Pa). The relation E/p is useful to calculate FWHM in order to estimate the temperature and number density of thermal electrons for argon mass of 6.4×10^{-26} kg.

In experiment ii, the number of secondary electrons production at the cathode induced by argon ions impact compensated the loss of electrons at the anode and there by enabled self-sustained discharge. To determine the breakdown threshold, the electric field distortion can be neglected, and the field can be assumed uniform and equal to the applied field. As with DC (and low-frequency) breakdown, higher values of pd require larger voltages to achieve breakdown, and at low pd there is again a sharp rise in breakdown voltage. If the long path explanation is considered then, the penetration of the discharge into the gap between the electrode and the insulator allows the discharge length to vary as required and the breakdown voltage stays close to the minimum value of 260 V.

In experiment iii, different velocities of the argon particles emission resulted in different Doppler shifts, the cumulative effect of which is the homogeneous line broadening. The following calculations are based on the assumption that the plasma between the two spherical electrodes is collisionless (this is reasonable because most of such electrostatic confinement fusion experiments are carried out at a pressure around 10^{-3} mbar where the mean free paths are in the order of the size of the machine). The temperature for different potentials was measured. For each applied potential, the wavelength resulted to the same peaks formation, around 420 ± 0.5 and 528 ± 0.5 nm. Moreover, for thermal plasmas with a gas temperature similar to the electron one, the mobility of ions is high and the impact approximation is also valid for ions,

being their contribution to the broadening also Lorentzian. The spectrum of lines emission from argon plasmas resulted in 4 peaks ranged between 467 and 469 nm comprise ions excitation (electronic transitions). While the fusor is in progress, the spectra intensity (counts) will change, and then it is possible to determine the temperature (ΔT) in the plasma, changing from 7 to 10 eV. While argon ions are moving a Maxwell-Boltzmann distance ($\Delta d = d - d_0$), there are photon emission with initial velocity (v_0) to final velocity (v_f) due to energy loss.

Analyzing the FWHM, it can be estimated for each temperature, $\Delta d = \lambda_2 - \lambda_1 \approx 0.20 \pm 0.1$ nm. Using the equations $d/d_0 = (1 - v/c)$, and $\Delta f = v/d_0$, then, the estimated electrons frequency is 2.1363 MHz. The distance (Δd) does not change significantly for each condition, which means that the temperature does not change significantly as function of the applied ΔV .

For typical fusor energy (MeV), the plasma temperature calculated ranged from 0.21 to 1.58 eV while the number density was estimated as $1.012 \times 10^{13} \text{ m}^{-3}$.

The number of electrons produced by secondary processes can be explained by Townsend coefficient (γ) which explains the increase of ion current during the increase of the voltage, followed by relaxed electric field. The γ depends on the constants A and B in the equation $Vb = B p d / \ln(Apd) - \ln[\ln(1 + 1/\gamma)]$, which assumes different values according to the plasma conditions.

ACKNOWLEDGEMENTS

The author would like to thank the European Fusion Education Network (FUSENET), the Eindhoven University of Technology (TU/e) by the magnificent opportunity and the Hotel NH Eindhoven Conference Centre Koningshof by the amazing accommodation.

REFERENCES

- Langmuir I. Positive ion currents from the positive column of Mercury arcs. *Science*, 1923;58(1502):290-1. <https://doi.org/10.1126/science.58.1502.290>
- Stenzel RL. (1997). FF. Chen, *Plasma Physics and Controlled Fusion*, 2 ed., Plenum Press, 1984.
- Kato K, Iizuka S. Analysis of Langmuir Probe Characteristics for Measurement of Plasma Parameters in RF Discharge Plasmas. *J Appl Math Phys*. 2016;4:1811-1836. <https://doi.org/10.4236/jamp.2016.49185>
- Rousseau A, Teboul E, Lang N, Hannemann M, Ropcke J. Langmuir probe diagnostic studies of pulsed hydrogen plasmas in planar microwave reactors. *J Appl Phys*. 2002;92(7):3463-71. <https://doi.org/10.1063/1.1497454>
- Masherov PE. A cylindrical langmuir probe primary probe holder size effect on the results of local plasma diagnostics. *Aerospace MAI J*. 2016;23(2):42-9.
- Masherov PE, Obukhov VA, Riaby VA, Savinov VP. International Symposium on Plasma Chemistry In 21st International Plasma Chemistry Society (IPCS). The Royal Australian Chemical Institute Incorporated [internet event] 2013 Aug 4-9; Cairns, Australia [cited year Month day]. Available at: <https://www.raci.org.au/events/event/21st-international-symposium-on-plasma-chemistry>
- Brockhaus A, Borchardt C, Engemann J. Langmuir probe measurements in commercial plasma plants. *Plasma Sources Sci Technol*. 1994;3(4):539-44. <https://doi.org/10.1088/0963-0252/3/4/011>
- Pramila, Patel JJ, Rajpal R, Hansalia CJ, Anitha VP, Sathyanarayana K. Solving the Capacitive Effect in the High-frequency sweep for Langmuir Probe in SYMPLE. *J Phys Conf Ser*. 2017; 823(1):1-6. <https://doi.org/10.1088/1742-6596/823/1/012019>
- Melzer A, Flohr R, Piel A. Comparison of probe measurements and emission spectroscopy in a radiofrequency discharge. *Plasma Sources Sci Technol*. 1995;4(3):424-31. <https://doi.org/10.1088/0963-0252/4/3/012>
- Masherov PE, Piskunkov AF, Riaby VA, Savinov VP, Yakunin VG. New Applications of Langmuir Probes. *Phys At Nucl*. 2017;80(11):1697-700. <https://doi.org/10.1134/S1063778817110114>
- Pieper JB, Goree J. Dispersion of Plasma Dust Acoustic Waves in the Strong-Coupling Regime. *Phys Rev Lett*. 1996;77(15):3137-240. <https://doi.org/10.1103/PhysRevLett.77.3137>
- Abe T, Oyama K-I. Langmuir Probe. In: Oyama K, Cheng CZ. An Introduction to Space Instrumentation. Tokyo, Japan: Terrapub 2013. <https://doi.org/10.5047/aisi.010>
- Johnson EO, Malter L. A floating double probe method for measurements in gas discharges. *Phys Rev*. 1950;80(1):58-68. <https://doi.org/10.1103/PhysRev.80.58>
- Pilling LS, Bydder EL, Carnegle DA. A computerized Langmuir probe system. *Rev Sci Instrum*. 2006;74(7):3341-3346. <https://doi.org/10.1063/1.1581362>
- Bilik N, Anthony R, Merritt BA, Aydil ES, Kortshagen UR. Langmuir probe measurements of electron energy probability functions in dusty plasmas. *J Phys D Appl Phys*. 2015;48(10):1-105204 (9pp). <https://doi.org/10.1088/0022-3727/48/10/105204>
- Lafleur T, Chabert P. Is collisionless heating in capacitively coupled plasmas really collisionless? *Plasma Sources Sci Technol*. 2015;24(4):1-10. <https://doi.org/10.1088/0963-0252/24/4/044002>
- Lafleur T, Chabert P, Booth JP. Electron heating in capacitively coupled plasmas revisited. *Plasma Sources Sci Technol*. 2014;23(3):1-12. <https://doi.org/10.1088/0963-0252/23/3/035010>
- Kechkar S. Experimental investigation of a low pressure capacitively-coupled discharge, Dublin. PhD Thesis [School of Physical Sciences] – Dublin City University; 2015.
- Riaby VA, Masherov PE, Savinov VP, Yakunin VG. RF plasma probe diagnostics: a method for eliminating measurement errors for Langmuir probes with bare protective shields. *J Phys Conf Ser*. 2018;958:1-14. <https://doi.org/10.1088/1742-6596/958/1/012006>
- Babu S. Investigation of structure observed in measured electron energy probability function in capacitively coupled oxygen discharge. NCPST 5th Radio Frequency Discharges Workshop; 2015 Jun 12; Dublin (Ireland).
- Park C, Pamidi S, Graber L. Boltzmann Analysis of Cryogenic He-H₂ Gas Mixtures as Dielectric Media for High-Temperature Superconducting Power Devices. *IEEE Trans Appl Supercond*. 2017;27(4):1-6. <https://doi.org/10.1109/TASC.2016.2637319>

22. Park C, Graber L, Pamidi S. The dielectric properties of gaseous cryogen mixtures of He, H₂, Ne, and N₂ in a temperature range of 50–80 K at pressures up to 2.0 MPa. *J Appl Phys.* 2017;21(8):1-13. <https://doi.org/10.1063/1.4976565>
23. Park C, Graber L, Cheetham P, Viquez JG, Kim CH, Pamidi S. A Versatile Modeling Technique for Predicting Dielectric Strength Improvements in Gas Mixtures for Superconducting Applications. *IEEE Trans Dielectr Electr Insul.* 2017;24(5):2755-64. <https://doi.org/10.1109/tdei.2017.006653>
24. Cheetham P, Kim W, Kim CH, Graber L, Rodrigo H, Pamidi S. Enhancement of Dielectric Strength of Cryogenic Gaseous Helium by Addition of Small Mol% Hydrogen. *IEEE Trans Appl Supercond.* 2017;27(4):1-5. <https://doi.org/10.1109/TASC.2016.2642539>
25. Korolov I, Donkó Z. Breakdown in hydrogen and deuterium gases in static and radio-frequency fields. *Phys Plasmas.* 2015;22(9):1-8. <https://doi.org/10.1063/1.4929858>
26. Demidov VI, Kudryatsev AA, Kurlyandskaya IP, Stepanova OM. Nonlocal control of electron temperature in short direct current glow discharge plasma. *Phys Plasmas.* 2014;21(9):1-5. <https://doi.org/10.1063/1.4896717>
27. Adams SF, Demidov VI, Bogdanov E, Koepke ME, Kudryatsev AA, Kurlyandskaya IP. Suprathermal electron energy spectrum and nonlocally affected plasma-wall interaction in helium/air micro-plasma at atmospheric pressure. *Phys Plasmas.* 2016;23(10):1-6. <https://doi.org/10.1063/1.4964721>
28. Lieberman MA, Lichtenberg AJ. *Principles of Plasma, Discharges and Material Processing.* 2 ed. Hoboken (NJ): Wiley; 2005.
29. Phelps AV, Petrović ZL. Cold-cathode discharges and breakdown in argon: surface and gas phase production of secondary electrons. *Plasma Sources Sci Technol.* 1999;8(3):R21-R44. <https://doi.org/10.1088/0963-0252/8/3/201>
30. Demidov VI, Adams SF, Kaganovich ID, Koepke ME, Kurlyandskaya IP. Measurements of low-energy electron reflection at a plasma boundary. *Phys Plasmas.* 2015;22(10):1-5. <https://doi.org/10.1063/1.4933002>
31. Pai P, Azar MT. Sub 3-micron gap microplasma FET with 50 V turn-on voltage. In *Proceedings of the 2014 IEEE 27th International Conference on Micro Electro Mechanical Systems (MEMS); 2014 January 26-30; San Francisco (CA): IEEE; 2014.* <https://doi.org/10.1109/MEMSYS.2014.6765601>
32. Loeb LB. *Basic processes of Gaseous Electronics.* Berkeley (CA): University of California Press; 1955.
33. Radjenović MR, Radjenović B. The role of the field emission effect in the deviations from the Paschen law. 28th ICPIG; 2007 Jul 15-20; Prague, Czech Republic: ICPIG; 2007.
34. Mesyats GA. Ectons and their role in plasma processes. *Plasma Phys Control Fusion.* 2005;47(5A):A109.
35. Marić D, Hartmann P, Malović G, Donkó Z, Petrović ZL. Measurements and modelling of axial emission profiles in abnormal glow discharges in argon: heavy-particle processes. *J Phys D Appl Phys.* 2003;36(21):2639-48. <https://doi.org/10.1088/0022-3727/36/21/007>
36. Marić D, Škoro N, Maguire PD, Mahony CMO, Malović G, Petrović ZL. On the possibility of long path breakdown affecting the Paschen curves for microdischarge. *Plasma Sources Sci Technol.* 2012;21(3):1-6. <https://doi.org/10.1088/0963-0252/21/3/035016>
37. Phelps AV, Petrović ZL. Cold-cathode discharges and breakdown in argon: surface and gas phase production of secondary electrons. *Plasma Sources Sci Technol.* 1999;8(3):R21-R44. <https://doi.org/10.1088/0963-0252/8/3/201>
38. Petrović ZL, Phelps AV. Oscillations of low-current electrical discharges between parallel-plane electrodes. I. dc discharges. *Phys Rev E.* 1993;47:2806-15. <https://doi.org/10.1103/PhysRevE.47.2806>
39. Marić D, Hartmann P, Malović G, Donkó Z, Petrović ZL. Measurements and modelling of axial emission profiles in abnormal glow discharges in argon: heavy-particle processes. *J Phys D Appl Phys.* 2003;35(21).
40. Paschen F. Ueber die zum Funkenübergang in Luft, Wasserstoff und Kohlensäure bei verschiedenen Drucken erforderliche Potentialdifferenz. *Annalen Der Physik.* 1889;273(5):69-75. <https://doi.org/10.1002/andp.18892730505>
41. Paschen F. *Annalen der Physik,* 1889;273(5):69-96.
42. Penning FM, Addink CCJ. The starting potential of the glow discharge in neon-argon mixtures between large parallel plates: I. Results. *Physica.* 1934;1(7-12):1007-27. [https://doi.org/10.1016/S0031-8914\(34\)80297-2](https://doi.org/10.1016/S0031-8914(34)80297-2)
43. Miller HC. Breakdown potential of neon below the Paschen minimum. *Physica.* 1964;30(11):2059-67. [https://doi.org/10.1016/0031-8914\(64\)90027-8](https://doi.org/10.1016/0031-8914(64)90027-8)
44. Auday G, Guillot PH, Galy J, Brunet H. Experimental study of the effective secondary emission coefficient for rare gases and copper electrodes. *J Appl Phys.* 1998;83(11):5917-21.
45. Lisovskiy VA, Yakovin SD, Yegorenkov VD. Low-pressure gas breakdown in uniform DC electric field. *J Phys D Appl Phys.* 2000;33(21):2722-30. <https://doi.org/10.1088/0022-3727/33/21/310>
46. Mariotti D, McLaughlin JA, Maguire P. Experimental study of breakdown voltage and effective secondary electron emission coefficient for a micro-plasma device. *Plasma Sources Sci Technol.* 2004;13(2):207-12. <https://doi.org/10.1088/0963-0252/13/2/003>
47. Charles C, Boswell RW, Takahashi K. Investigation of radiofrequency plasma sources for space travel. *Plasma Phys Control Fusion.* 2012;54(12):124021. <https://doi.org/10.1088/0741-3335/54/12/124021>
48. Liu W, Zhang D, Kong F. The Impact of Electrode Configuration on Characteristics of Vacuum Discharge Plasma. *Plasma Sci Technol.* 2012;14(2):122. <https://doi.org/10.1088/1009-0630/14/2/08>
49. Radmilović-Radjenović M, Matejčić Š, Klas M, Radjenović B. The role of the field emission effect in direct-current argon discharges for the gaps ranging from 1 to 100 μm. *J Phys D Appl Phys.* 2013;46(1):015302. <https://doi.org/10.1088/0022-3727/46/1/015302>
50. Mohammed SJ, Khalaf MK, Majeed MA, Jasem HE. Experimental study on the effect of longitudinal magnetic field on Townsend discharge characteristics in low pressure argon gas. *Int J Adv Appl Sci.* 2017;4(2):91-95. <https://doi.org/10.21833/ijaas.2017.02.016>
51. Gainutdinov RKh, Mutygoullina AA, Khamadeev MA, Petrova AS. Unstable vacuum and spectrum of atoms with a superheavy nucleus. *J Phys Conf Ser.* 2013;478(1):012019. <https://doi.org/10.1088/1742-6596/478/1/012019>
52. Gainutdinov RKh, Mutygoullina AA, Petrova AS. Natural spectral-line broadening in atoms with unstable nuclei. *J Phys Conf Ser.* 2015;613(1):012003. <https://doi.org/10.1088/1742-6596/613/1/012003>
53. Stenzel RL, Gruenwald J, Fonda B, Ionita C, Schrittwieser R. Transit time instabilities in an inverted fireball. II. Mode jumping and nonlinearities. *Phys Plasmas.* 2011;18(1):012105. <https://doi.org/10.1063/1.3533440>

54. Stenzel RL, Gruenwald J, Fonda B, Ionita C, Schrittwieser R. Transit time instabilities in an inverted fireball. I. Basic properties. *Phys Plasmas*. 2011;18(1):012104. <https://doi.org/10.1063/1.3533437>
55. Gruenwald J, Frohlich M. Coupling of transit time instabilities in electrostatic confinement fusion devices. *Phys Plasmas*. 2015;22:070701. <https://doi.org/10.1063/1.4926820>
56. Devia DM, Rodriguez-Restrepo LV, Restrepo-Parra E. Methods Employed in Optical Emission Spectroscopy Analysis: a Review. *Ing Cienc*. 2015;11(21):239-267. <https://doi.org/10.17230/ingciencia.11.21.12>
57. Cadwell L, Huwel L. Time-resolved emission spectroscopy in lasergenerated argon plasmas—determination of Stark broadening parameters. *J Quant Spectrosc Ra*. 2004;83(3-4):579-98. [https://doi.org/10.1016/S0022-4073\(03\)00106-7](https://doi.org/10.1016/S0022-4073(03)00106-7)
58. Hutchinson IH. *Principles of Plasma Diagnostics*. 2 ed. Cambridge (UK): Cambridge University Press; 2002. <https://doi.org/10.1017/CBO9780511613630>
59. Allen LH. *Astrophysics: The Atmosphere of the Sun and Stars*. 2 ed. New York (NY): Ronald Press; 1963.
60. Duguet T, Fournée V, Dubois J, Belmonte T. Study by optical emission spectroscopy of a physical vapour deposition process for the synthesis of complex AlCuFe(B) coatings. *Surf Coat Tech*. 2010;205(1):9-14. <https://doi.org/10.1016/j.surfcoat.2010.05.030>
61. Qayyum A, Ikram M, Zakauallah M, Waheed A, Murtaza G, Ahmad R, Majeed A, Khattak NAD, Mansoor K, Chaudhary KA. Characterization of argon plasma by use of Optical Emission Spectroscopy and Langmuir Probe Measurements. *Int J Mod Phys B*. 2003;17(14):2749-59. <https://doi.org/10.1142/S0217979203018454>
62. Bibinov NK. et al., *Plasma Sources Sci Technol*. 2005;14:109. Tuske O. et al., *Rev. Sci. Instrum.*, 2004;75:1529.
63. Foissac C, Kristof J, Annusova A, Veis P, Supiot P. Spectroscopic diagnostics and modelling of a N₂-Ar mixture discharge created by an RF helical coupling device: I. Kinetics of N₂(B₃Π_g) and N₂(C₃Π_u) states. *Plasma Sources Sci Technol*. 2012;21(5):055021. <https://doi.org/10.1088/0963-0252/21/5/055021>
64. Zhu X, Pu Y-K, Celik Y, Siepa S, Schungel E, Luggenholscher D, Czarnetzki U. Possibilities of determining non-Maxwellian EEDFs from the OES line-ratios in low-pressure capacitive and inductive plasmas containing argon and krypton. *Plasma Sources Sci Technol*. 2012;21(2):024003. <https://doi.org/10.1088/0963-0252/21/2/024003>
65. Tanışlı M, Şahin N. Optical characteristics for capacitively and inductively radio frequency discharge and post-discharge of helium. *Phys Plasmas*. 2016;23(1):013513. <https://doi.org/10.1063/1.4940783>
66. Lock EH, Petrova TB, Petrov GM, Boris DR, Walton SG. Electron beam-generated Ar/N₂ plasmas: The effect of nitrogen addition on the brightest argon emission lines. *Phys Plasmas*. 2016;23(4):043518. <https://doi.org/10.1063/1.4946880>
67. Zhu X, Y.-K. Pu, Y. Celik, S. Siepa, E. Schungel, D. Luggenholscher, and U. Czarnetzki, *Plasma Sources Sci Technol*. 2012;21:024003.
68. Zhu X, Pu Y. *J Phys D Appl Phys*. 2010;43:403001 Boffard JB, Jung RO, Lin CC, Wendt AE. *Plasma Sources Sci Technol*. 2010;19:065001.
69. [69] Bogaerts A, Gijbels R, Vlcek J. Modeling of glow discharge optical emission spectrometry: Calculation of the argon atomic optical emission spectrum. *Spectrochim Acta Part B*. 1998;53(11):1517-26. [https://doi.org/10.1016/S0584-8547\(98\)00139-6](https://doi.org/10.1016/S0584-8547(98)00139-6)
70. Bogaerts A, Gijbels R. Modeling of metastable argon atoms in a direct-current glow discharge. *Phys Rev A*. 1995;52(5):3743-51. <https://doi.org/10.1103/PhysRevA.52.3743>
71. Zhu X-M, Pu Y-K. Optical emission spectroscopy in low-temperature plasmas containing argon and nitrogen: determination of the electron temperature and density by the line-ratio method. *J Phys D Appl Phys* 2010;43(40):403001-25. <https://doi.org/10.1088/0022-3727/43/40/403001>
72. Zhu X, Pu Y-K, Celik Y, Siepa S, Schungel E, Luggenholscher D, Czarnetzki U, *Plasma Sources Sci Technol*. 2012;21(2):024003. <https://doi.org/10.1088/0963-0252/21/2/024003/meta>
73. Zhu X, Pu Y-K. Optical emission spectroscopy in low-temperature plasmas containing argon and nitrogen: determination of the electron temperature and density by the line-ratio method. *J Phys D Appl Phys*. 2010;43(40):403001.
74. Boffard JB, Jung RO, Lin CC, Wendt AE. *Plasma Sources Science and Technology Optical emission measurements of electron energy distributions in low-pressure argon inductively coupled plasmas*. *Plasma Sources Sci Technol*. 2010;19(6):065001. <https://doi.org/10.1088/0963-0252/19/6/065001>
75. Lock EH, Petrova TzB, Petrov GM, Boris DR, Walton SG. Electron beam-generated Ar/N₂ plasmas: The effect of nitrogen addition on the brightest argon emission lines. *Physics of Plasmas* 2016;23:043518.
76. Dasgupta A, Blaha M, Giuliani JL, Electron-impact excitation from the ground and the metastable levels of Ar I. *Phys Rev A*. 1999;61(1):012703. <https://doi.org/10.1103/PhysRevA.61.012703>
77. Allard N, Kielkopf J. The effect of neutral non resonant collisions on atomic spectral lines. *Rev Mod Phys*. 1982;54:1103-82. <https://doi.org/10.1103/RevModPhys.54.1103>
78. Ali AW, Giem HR. Theory of resonance broadening of spectral lines by atom-atom impacts. *Phys Rev*. 1965;140(4A):1044-9. <https://doi.org/10.1103/PhysRev.140.A1044>. Erratum in: *Phys Rev*. 1966;144(1):366. <https://doi.org/10.1103/PhysRev.144.366>
79. Ali AW, Giem HR. Theory of resonance broadening of spectral lines by atom-atom impacts. *Phys Rev*. 1965;140(4A):1044-9. <https://doi.org/10.1103/PhysRev.140.A1044>
80. Nikiforov AY, Leys C, Gonzalez MA, Walsh JL. Electron density measurement in atmospheric pressure plasma jets: Stark broadening of hydrogenated and non-hydrogenated lines. *Plasma Sources Sci Technol*. 2015;24(3):034001-18. <https://doi.org/10.1088/0963-0252/24/3/034001>
81. Shafir G, Zolotukhin D, Godyak V, Shlapakovski A, Gleizer S, Slutsker Y, Gad R, Bernshtam V, Ralchenko Y, Krasik YE. Characterization of inductively coupled plasma generated by a quadruple antenna. *Plasma Sources Sci Technol*. 2017;26(2):025005, <https://doi.org/10.1088/1361-6595/aa5300>
82. Fox-Lyon N, Oehrlein GS, Godyak V. Effect of surface derived hydrocarbon impurities on Ar plasma properties. *J Vac Sci Technol A*. 2014;32(3):030601. <https://doi.org/10.1116/1.4867158>
83. Jogi I, Raud J, Hein K, Laan M. Spectral characterization of medium-pressure RF discharge in argon-oxygen mixture. *J Phys D Appl Phys*. 2014;47(33):335206. <https://doi.org/10.1088/0022-3727/47/33/335206>
84. K-I. Oyama, Y. W. Hsu, G. S. Jiang, W. H. Chen, C. Z. Cheng, H. K. Fang and W. T. Liu, *Rev. Sci. Instrum*. 86, 084703 (2015). D. Voloshina, A. Kovalev, Y. Mankelevich, O. Proshina, T. Rakhimova, and A. Vasilieva, *Eur. Phys. J. D* 69(1), 23 (2015).

85. Tejero-del-Caz A, Palop JIF, Diaz-Cabrera JM, Ballesteros J, Radial-to-orbital motion transition in cylindrical Langmuir probes studied with particle-in-cell simulations. *Plasma Sources Sci Technol.* 2016;25(1):01LT03. <https://doi.org/10.1088/0963-0252/25/1/01LT03>
86. Braithwaite NSJ. Introduction to gas discharges. *Plasma Sources Sci Technol.* 2000;9(4):517-27. <https://doi.org/10.1088/0963-0252/9/4/307>
87. Bustos A, Juarez AM, de Urquijo J, Muñoz M. An automated Langmuir probe controller for plasma characterization. *Meas Sci Technol.* 2016;27(8):087002. <https://doi.org/10.1088/0957-0233/27/8/087002>
88. Abe T, Oyama K. An Introduction to Space Instrumentation. Tokyo, Japan: Terrapub; 2013. 63-75 p.
89. Chung P, Talbot L, Touryan KJ. Electrical probes in stationary and flowing plasmas. New York (NY): Springer; 1975.
90. Braithwaite NSJ, Franklin RN. Reflections on electrical probes. *Plasma Sources Sci Technol.* 2009;18(1):014008. <https://doi.org/10.1088/0963-0252/18/1/014008>
91. Itagaki N, Iwata S, Muta K, Yonesu A, Kawakami S, Ishii N, Kawai Y. Electron-Temperature Dependence of Nitrogen Dissociation in 915 MHz ECR Plasma. *Thin Solid Films* 2003;435(1-2):259-63. [https://doi.org/10.1016/S0040-6090\(03\)00395-X](https://doi.org/10.1016/S0040-6090(03)00395-X)
92. Yong-ik S, Lim HB, Houk RS, Diagnostic Studies of Low-Pressure Inductively Coupled Plasma in Argon Using a Double Langmuir Probe. *J Anal At Spectrom.* 2002;17(6):565-9. <https://doi.org/10.1039/b110219m>
93. Radmilović-Radjenović M, Lee JK, Iza F, Park GY. Particle-in-cell simulation of gas breakdown in microgaps. *J Phys D Appl Phys.* 2005;38(6):950-4. <https://doi.org/10.1088/0022-3727/38/6/027>
94. Radmilović-Radjenović M, Radjenović B. The influence of ion-enhanced field emission on the high-frequency breakdown in microgaps. *Plasma Sources Sci Technol.* 2007;16(2):337-40. <https://doi.org/10.1088/0963-0252/16/2/017>
95. Bekkara MF, Benmimoun Y, Tilmatine A, Miloudi K, Flazi S. An effective approach for designing a low pressure DC glow discharge plasma reactor. *J Electrostat.* 2017;88:225-31. <https://doi.org/10.1016/j.elstat.2017.01.004>
96. Wais SI, Mohammed RY, Yousif SO. Influence of Axial Magnetic Field on the Electrical Breakdown and Secondary Electron Emission in Plane-Parallel Plasma Discharge. *World Acad Sci Eng Technol.* 2011;5(8):1226-31. <https://doi.org/10.5281/zenodo.1333588>
97. Raizer YP, Gas Discharge Physics. New York (NY): Springer; 1997.
98. Petrović ZL, Škoro N, Marić D, Mahony CMO, Maguire PD, Radmilović-Radjenovic M, Malović G. Breakdown, scaling and volt-ampere characteristics of low current micro-discharges. *J Phys D Appl Phys* 2008;41(19):194002. <https://doi.org/10.1088/0022-3727/41/19/194002>
99. Hutchinson IH. Principles of Plasma Diagnostics. 2 ed. New York (NY): Cambridge University Press; 2002. 264-265 p.
100. Griem, HR. (1974) Spectral line broadening by plasmas. New York (NY): Academic Press; 1974.
101. Yubero C, Rodero A, Dimitrijevic M, Gamero A, García MC. Gas temperature determination in an argon non-thermal plasma at atmospheric pressure from broadenings of atomic emission lines. *Spectrochim Acta Part B.* 2017;129:14-20. <https://doi.org/10.1016/j.sab.2017.01.002>
102. Griem HR. Plasma spectroscopy. New York (NY): McGraw-Hill; 1964.
103. Griem HR. Spectral line broadening by plasmas. New York (NY): Academic Press; 1974.
104. Kunze HJ. Introduction to plasma spectroscopy. Berlin: Springer; 2009.
105. Lieberman MA, Lichtenber AJ. Principles of Plasma Discharges and Materials Processing. 2005; (2), p. 128.
106. Hutchinson IH. Principles of Plasma Diagnostics. 2002; 2 ed. Cambridge University Press, New York.
107. Lieberman, Michael A.; Lichtenberg, Allan J. (2005). Principles of plasma discharges and materials processing (2nd ed.). Hoboken, N.J.: Wiley-Interscience.